NANO LETTERS

2008
Vol. 8, No. 10
3102-3108

Coherent Phonon Anisotropy in Aligned Single-Walled Carbon Nanotubes

Keiko Kato,[†,⊗] Kunie Ishioka,[†] Masahiro Kitajima,[*,†,‡] Jie Tang,[§] Riichiro Saito,[∥] and Hrvoje Petek[#,%]

Advanced Nano Characterization Center, National Institute for Materials Science, Tsukuba, Ibaraki 305-0047, Japan, Department of Applied Physics, School of Applied Science, National Defense Academy of Japan, Yokosuka, Kanagawa, 239-8686, Japan, Innovate Materials Engineering Laboratory, National Institute for Materials Science, Tsukuba, Ibaraki 305-0047, Japan, Department of Physics, Tohoku University, Sendai 980-8578, Japan, Department of Physics and Astronomy, University of Pittsburgh, Pittsburgh, Pennsylvania 15260, and Donostia International Physics Center DIPC, P. Manuel de Lardizabal 4, 20080 San Sebastian, Spain

Received April 28, 2008; Revised Manuscript Received July 28, 2008

ABSTRACT

By time-resolved reflectivity measurements with sub-10 fs laser pulses at 395 nm, the coherent phonons of aligned bundles of single-walled carbon nanotubes are observed for various polarization directions of the pump and probe pulses. In the isotropic reflectivity measurement, we observe the radial breathing modes, G, and even D modes, while in the anisotropic reflectivity mode, only the G mode appears. A complex polarization dependence of the G band phonon amplitude in the isotropic reflectivity is explained by the superposition of G band phonons with different symmetries.

Quasi-one-dimensional carbon nanotubes (CNTs), rolled-up graphene sheets, have attracted much attention because of their unique electronic and structural properties. Quantum confinement effects have significant influence on their physical properties, such as ballistic transport,[1] exciton binding,[2−4] and Kohn anomaly.[5,6] For an isolated single-walled carbon nanotube (SWCNT) or aligned SWCNT bundle samples, the photoresponse strength in absorption,[7] photoluminescence,[8,9] photoconductivity,[10] and polarized resonance Raman measurements[11,12] depend strongly on the polarization of light with respect to the CNT axis corresponding to the strong (weak) optical transition moment for the parallel (perpendicular) polarization alignment.[13] The anisotropic optical properties, which arise from the quasi-one-dimensional nature of CNTs, may lead to important applications of CNTs as optical antennas.[14]

Another important optical property of CNTs is a very fast response of the photoexcited carriers. The carrier-scattering processes, such as electron−electron (e−e), electron−phonon (e−ph), or carrier-impurity, which are important for the transport properties of CNTs, have been widely investigated by photoluminescence[8,9] and photoconductivity measurements.[10] Because of the high mobility of carriers in graphitic materials and the rapid energy relaxation of the photoexcited carriers, CNTs can respond to an outer field even at terahertz frequencies.[15] The scattering properties of high-energy photoexcited carriers are determined by emission of optical phonons on time scales less than 100 fs through strong electron− or exciton−phonon interactions. In the case of CNTs, not only the zone-center phonon modes (the G band at around 1580 cm^{-1} and the radial breathing mode (RBM) at 100−200 cm^{-1}) but also the zone-boundary phonon (G′ band at around 2700 cm^{-1}) are known to be influenced by strong electron−phonon interaction.[16] The G′ band, which has a strong Raman response, appears through a double-resonance Raman process involving two-phonon scattering.[17] When one of the phonon scattering processes in the double resonance is substituted by defect-induced elastic scattering, the D band appears at around 1350 cm^{-1} in defective CNTs and graphite.

In the case of the G band, the curvature of a cylindrical CNT splits the degenerate E_{2g} symmetry G band of graphite

* Corresponding author. Phone: +81-46-841-3810. Fax: +81-46-844-5912. E-mail: kitaji@nda.ac.jp.
† Advanced Nano Characterization Center, National Institute for Materials Science.
‡ National Defense Academy of Japan.
§ Innovate Materials Engineering Laboratory, National Institute for Materials Science.
∥ Tohoku University.
University of Pittsburgh.
% Donostia International Physics Center DIPC.
⊗ Present address: NTT Basic Research Laboratories, Nippon Telegraph and Telephone Corporation.

10.1021/nl801200p CCC: $40.75
Published on Web 09/13/2008

into the higher (G^+) and lower (G^-) frequency modes. In the semiconducting CNTs, the G^+ (G^-) mode corresponds to longitudinal optic LO (transverse optic, TO) phonon mode, while in the metallic CNTs, the G^+ (G^-) mode corresponds to TO (LO) phonon mode. This reversal happens because of the softening of the LO phonon mode in metallic CNTs through the interaction with free electrons near the Fermi level (Kohn anomaly[5,6]). Because of the chirality dependent electron−phonon matrix element for the LO and TO phonon modes, the relative Raman intensity of the G^+ and G^- bands depends on the nanotube structure.[6,18] Moreover, for each G^+ or G^- band, the periodic boundary condition in the circumferential direction of a CNT defines the angular momentum of vibrational motion along the nanotube axis of 0, 1, and 2, corresponding to the A, E_1, and E_2 symmetry Raman active phonon modes.[19] Thus, we expect six different G band phonon modes in resonance Raman spectra, which can in principle be observed by polarized Raman spectroscopy.[19] In fact, in the previous polarized Raman spectra, these phonon modes could be analyzed into separate Lorentzian peaks.[12,20−22] For a particular geometry, Raman measurements for aligned nanotubes can selectively detect only E_1 or E_2 symmetry phonons.[19] Because the Raman cross section of the A symmetry G band mode is much stronger than those of the E symmetry modes and the alignment of CNT bundles is not always perfect, the selection of only E_1 or E_2 symmetry phonons is difficult to attain in polarized Raman spectroscopy.

Coherent phonon spectroscopy has the possibility of separating the A and E symmetry phonons by the choice of the excitation and detection geometries.[23,24] In general, we can choose the polarization of the excitation light with respect to the axis of the aligned CNTs. Moreover, we can analyze the reflected probe light in a transient reflectivity measurement into components parallel ($R_{//}$) and perpendicular ($R_\perp$) to the polarization of the pump. The sum ($R_{//} + R_\perp$) of the two signals in such a measurement gives the isotropic response, while the difference ($R_{//} - R_\perp$) gives the anisotropic response. The purely isotropic response could be obtained by recording the reflected light for 45° angle between the pump and the probe polarizations.

We have performed measurements on aligned CNTs for various angles between the pump polarization and the alignment axis while detecting either the $R_{//} + R_\perp$ or the $R_{//} - R_\perp$ components. Henceforth, we will refer to the former as the transient reflectivity and the latter as the electro-optic (EO) sampling configurations. In both measurements, the polarized laser excitation with a pulsed duration shorter than the period of phonon oscillation excited coherent phonon oscillations with different symmetries; the phonon oscillations in turn modulate the optical susceptibility and therefore the refractive index.[23,25,26] A symmetry phonons induce an isotropic change of the index, while E symmetry phonons induce a birefringent (ellipsoidal) change of the index.[25,26] In the transient reflectivity measurement, both the isotropic and the birefringent modulations of the index are detected through the measurement of $R_{//} + R_\perp$. The EO sampling measurement, however, cancels the isotropic index change by the A symmetry phonons while retaining the birefringent change by the E symmetry phonons. Such polarization sensitive measurements allow selective coherent phonon spectroscopy of either A or E symmetry phonons.

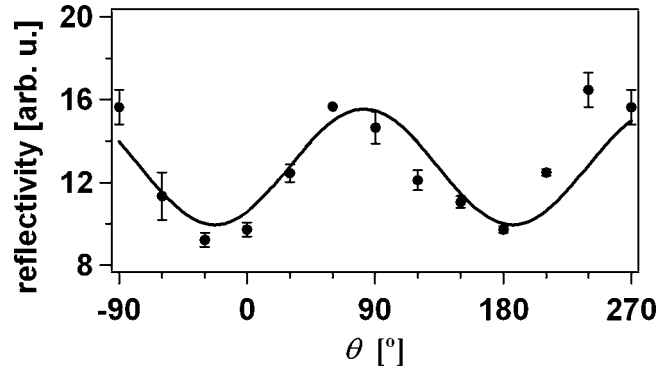

Figure 1. Polarization dependence of the sample reflectivity. Solid circles are experimental results plotted as a function of the angle (θ) between the laser polarization and the axis of CNTs. The solid line is a fit to the $\cos(2\theta)$ function.

So far, there have been several published reports on coherent phonons in SWCNTs.[27,28] By resonant excitation of specific SWCNTs with a tunable laser source with 50 fs pulse, Lim et al. observed the RBM oscillation in SWCNTs samples.[28] Gambetta et al., who employed resonant sub-10 fs visible laser excitation, observed both the RBM and the G band mode oscillations.[27] They observed the anharmonic coupling between the RBM and the G band modes through the modulation of the G mode frequency synchronously with the slower RBM oscillation. The randomly oriented samples used in the previous experiments, however, prevented the polarization dependence of signals and the symmetry assignment for the G band to be performed.

In this communication, we present a transient reflectivity and EO sampling study of the ultrafast dynamics of coherent phonons in aligned bundles of SWCNTs. With laser pulses shorter than the period of C−C stretching mode (21 fs), we are able to observe the coherent oscillations of the RBM, G, and even D modes in the transient reflectivity geometry, while we observe only the G mode in the EO sampling geometry.[24,29] By rotating the polarization direction of the pump and probe pulses independently, we investigate the antenna effect, which gives a large optical absorption matrix element for the parallel polarization and the isotropic (anisotropic) electron−phonon interaction for the RBM (G) band phonon. Although our observation does not cover all of the possible geometries and polarization directions, the present data suggest superposition of the G band phonons of different symmetries.

Pump−probe time-resolved reflectivity measurements were carried out under ambient conditions with sub-10 fs UV laser pulses at 395 nm. The excitation pulses were produced by frequency doubling of light from a 65 MHz Ti:sapphire laser oscillator.[23] The linearly polarized pump and probe pulses were focused by a 50 mm focal-length mirror to a 10 μm spot on the sample respectively with angles of 20° and 5° from the surface normal. The pump power could be varied up to a maximum of 50 mW, while the probe

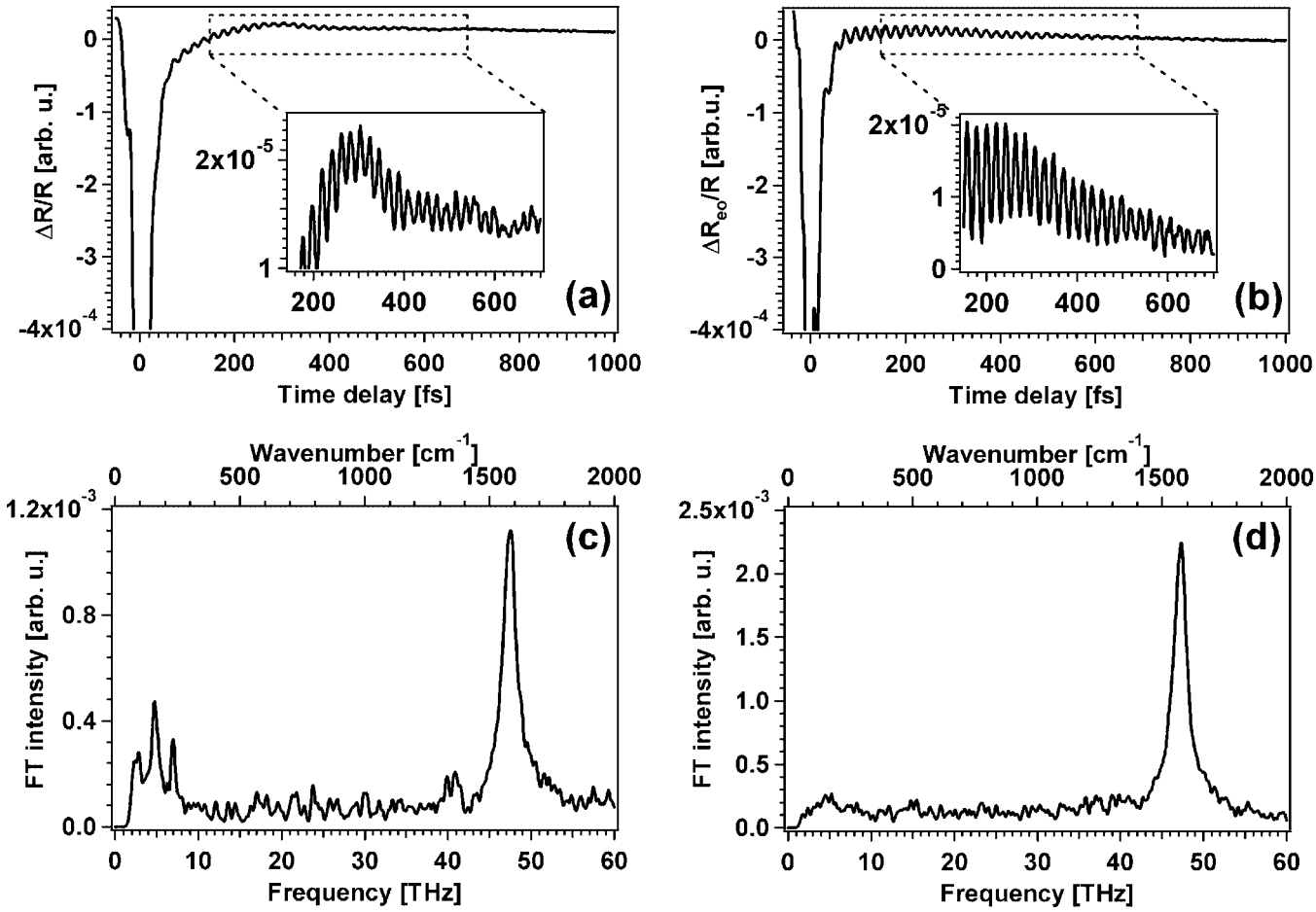

Figure 2. Time-resolved reflectivity of SWCNTs taken with the (a) transient reflectivity and (b) EO sampling. The inset is the enlarged signal for the oscillatory components. FT spectrum of the time-resolved reflectivity of SWCNTs taken with the (c) transient reflectivity measurement and (d) EO sampling.

power was kept below 3 mW. For the detection of all Raman-active phonon modes in SWCNTs, the transient reflectivity scheme was chosen, while for the nontotally symmetric (E_1 and E_2 symmetry) phonon modes, the EO sampling was chosen. In the transient reflectivity measurement, the intensity of the probe beam before and after reflection from the sample was measured with a pair of PIN photodiodes, and the difference between the signal and the reference photocurrents (ΔR) was measured as a function of the pump−probe delay. In the EO sampling, the probe beam, which is 45° polarized with respect to the optical plane, is decomposed into polarization components parallel ($R_{//}$) and perpendicular ($R_\perp$) to the optical plane after the reflection from the sample. Their difference $\Delta R_{eo} = R_{//} - R_\perp$ is measured as a function of the pump−probe delay. The differential current (ΔR or ΔR_{eo}) was amplified by a preamplifier with a band-pass filter set to transmit simultaneously the RBM and the G mode signals. The amplified signal was digitized and recorded with a digital oscilloscope. The differential current (ΔR or ΔR_{eo}) was normalized to $\Delta R/R$ (or $\Delta R_{eo}/R$) where R is the reflectivity without the pump pulse.

The sample used in this study consists of SWCNT bundles synthesized by the laser ablation method and purified by reflux in hydrogen peroxide and filtration. A clean hydrophilic glass slide was immersed vertically into the SWCNT/water suspension, and a self-assembled SWCNT film was formed on the slide.[30] The direction of SWCNTs was evaluated optically, as well as by transmission electron microscopy and polarized Raman spectroscopy.[30]

The reflectivity of the probe pulse from aligned SWCNTs shows a polarization dependence that can be used to define the direction of the alignment. The reflectivity of the probe pulse, without pump laser, is plotted in Figure 1 as a function of the angle (θ) between the laser polarization and the axis of SWCNTs. As expected from the previous work,[31,32] the polarization dependence of reflection shows a $\cos(2\theta)$ dependence with a minimum (maximum) when the polarization direction of the laser is parallel (perpendicular) to the axis of SWCNTs. This result is consistent with the antenna effect.[13]

After excitation of SWCNTs by the pump light, we can observe the ensuing carrier and coherent phonon dynamics through the delay-dependent changes in the amplitude of the reflected probe light. Figure 2a,b shows the experimental results for the time-resolved reflectivity of SWCNTs taken in the transient reflectivity measurement and EO sampling geometries, respectively. In both part a and part b of Figure 2, the transient photoinduced reflectivity consists

of two components. The first component is the initial, nonoscillatory response due to the excitation and the subsequent relaxation of excited carriers, while the second component is the oscillatory signal due to the coherent lattice vibrations.

To extract the oscillation frequencies, the Fourier transform (FT) of the oscillatory $\Delta R/R$ (Figure 2c) and $\Delta R_{eo}/R$ (Figure 2d) signals are obtained numerically. The FT spectrum obtained by the transient reflectivity measurement (Figure 2c) shows that the coherent phonon response can be separated into three frequency regions, (1) low-frequency (<10 THz), (2) 1350 cm^{-1} (40 THz), and (3) 1560−1580 cm^{-1} (47 THz), while that obtained by the EO sampling (Figure 2d) shows only the highest frequency component.

The multiple peaks in the low-frequency region correspond to RBMs of SWCNTs with different diameters (Figure 2c). Because they are totally symmetric, RBMs can be detected only in the transient reflectivity.[11] From the known dependence of the RBM frequency on the radius of SWCNTs,[2] we can conclude the signal originates from SWCNTs with diameters of 1.0(1), 1.4(2), and 1.6(2) nm. According to the Kataura plot,[33] which shows the relationship between transition energy and the diameter of SWCNTs, the 395 nm light resonantly excites the E_{22}^S, E_{11}^M, E_{33}^S, and E_{44}^S transitions.

The small peak at 40 THz can be observed only in the transient reflectivity (Figure 2c). On the basis of the published Raman spectra of SWCNTs,[17,34] we assign it the D mode. Defects appear to make it possible to observe the coherent D mode phonons only in the transient reflectivity geometry.

The strongest peak in the FT spectra at 47 THz is the G mode.[11] The G mode can have contribution only from the *E* symmetry modes in the EO sampling (Figure 2d) and from both the *A* and the *E* symmetry modes in the transient reflectivity (Figure 2c). The spectral resolution in the coherent phonon spectroscopy is determined by the dephasing time of a coherent phonon. In our CNT bundle sample, the dephasing can have contributions from interaction between tubes, defects, and the excitation of an electron into the higher energy states,[35] leading to the short dephasing time of phonons. In fact, the coherent G phonon modes dephase in 350 fs or less. The fast dephasing time causes spectral broadening in the FT spectra, restricting the frequency resolution and making it difficult to resolve the *A*, E_1, and E_2 symmetry components of the G band.

Because of the antenna effect, phonon amplitudes of all modes depend on the laser polarization with respect to the axis of CNTs. When both the pump and the probe polarizations are parallel to the axis of SWCNTs, both the RBM and the G mode have higher intensity than when they are perpendicular, as shown in Figure 3. Consistent with resonant Raman spectra, Figure 3 indicates that the antenna effect also dominates the generation of coherent phonons. If we had a better aligned sample, we could get more pronounced polarization dependence as found in polarized Raman spectroscopy.[12,36]

In Figure 4, we show the main result of our experiment, namely, the transient reflectivity measurement of SWCNTs

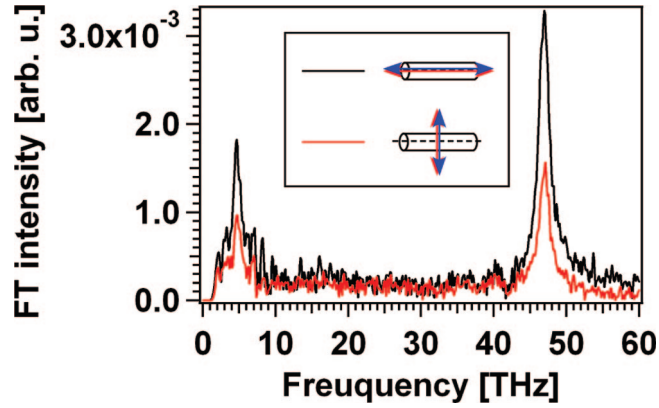

Figure 3. FT spectrum of the time-resolved reflectivity of SWCNTs when both the pump and the probe polarizations are parallel (black) or perpendicular (red) to the axis of SWCNTs.

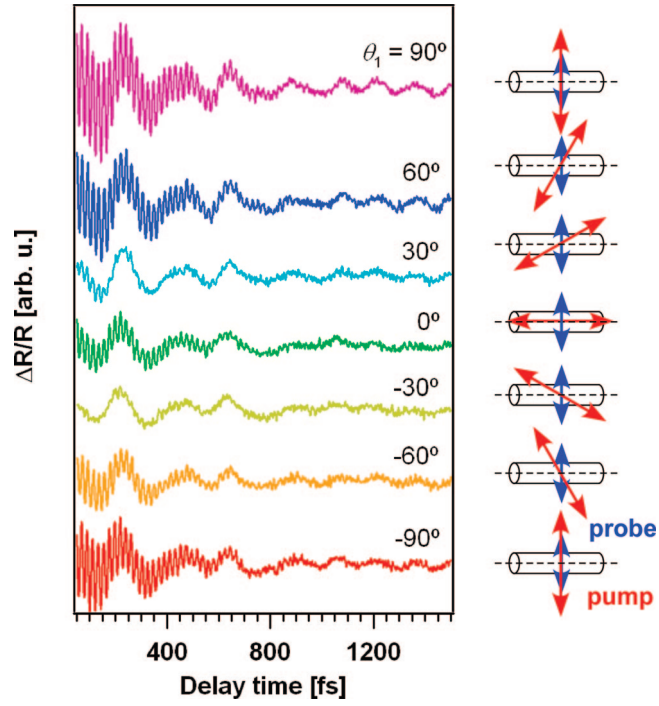

Figure 4. Time-resolved measurements of $\Delta R/R$ taken by rotating the polarization direction of the pump laser (red). The polarization direction of probe laser (blue) is set to be perpendicular to the axis of CNTs.

as a function of the angle θ_1 between the polarization of the pump laser angle and the axis of SWCNTs. The angle θ_1 was rotated, while the polarization of the probe laser was set to be perpendicular to the axis of SWCNTs. In Figure 4, the G mode component amplitude is nearly zero at $\theta_1 = -30°$ and 30° while the RBMs appear at all angles. In order to make the polarization dependence of each oscillatory component clear, the corresponding FT spectra are shown in Figure 5a. The amplitude of the G mode is modulated from maxima at $\theta_1 = -90°$ and 90° to minima at $\theta_1 = -30°$ and 30°. Because of the one-dimensional structure of SWCNTs, the polarization dependence should have mirror symmetry at $\theta_1 = 0°$. Because of the degradation of the sample during the measurement, however, the intensity of FT spectrum does not have the complete mirror symmetry

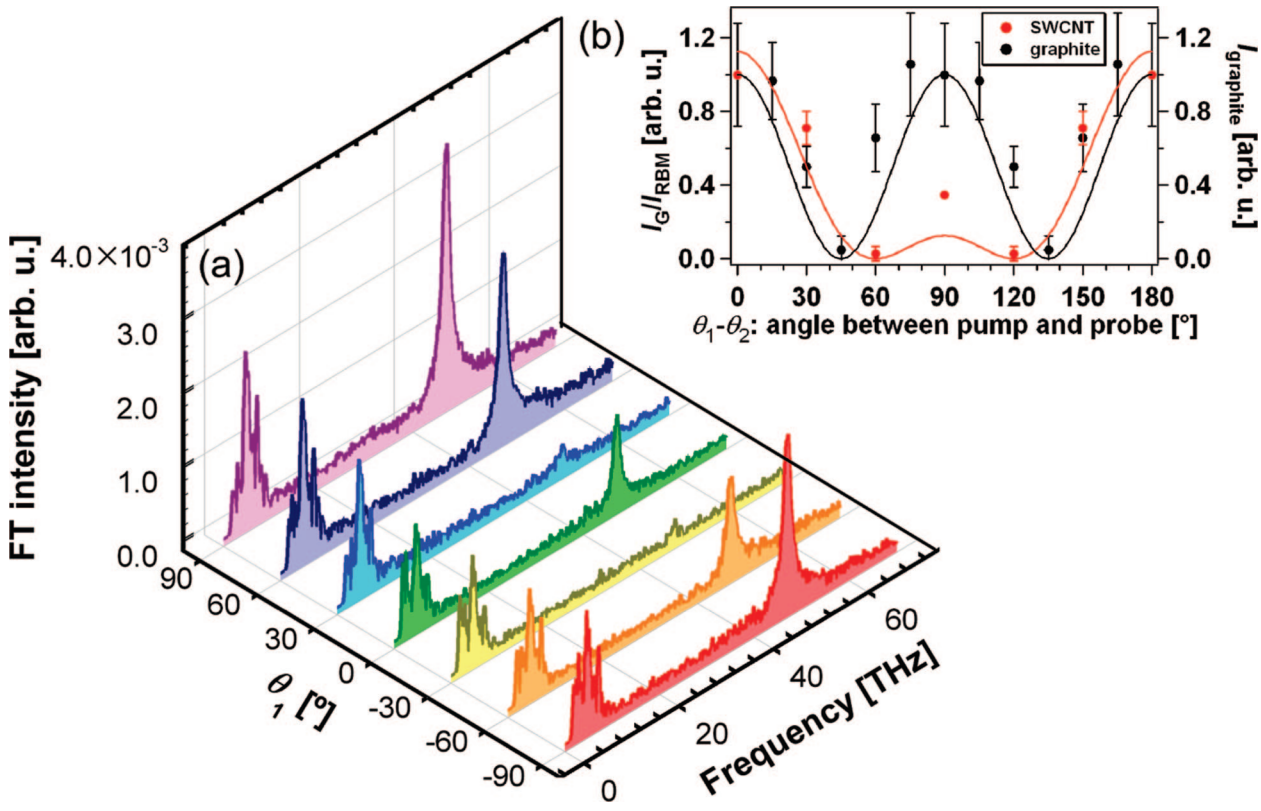

Figure 5. (a) FT spectrum of $\Delta R/R$ in Figure 4. The color of each plot corresponds to the FT spectrum with the same color shown in Figure 4. (b) Solid red circles give the ratio of the integrated intensity of the G mode and RBM, I_G/I_{RBM}, is plotted as a function of the angle between pump and probe. The solid red line is the fitting result with $|\alpha + \beta \cos(2(\theta_1 - \theta_2))|^2$ where $\alpha/\beta = 0.5$. For comparison, solid black circles give the polarization dependence of graphite as a function of the angle between the pump and the probe. The solid black line is the fitting result for graphite with $|\cos(2(\theta_1 - \theta_2))|^2$.

at $\theta_1 = 0°$. In order to remove this artifact, the ratio between the integrated intensities of the G mode and those of the RBM, I_G/I_{RBM}, is plotted as a function of $\theta_1 - \theta_2$, where θ_2 is the polarization angle between the probe laser and the axis of SWCNTs, as shown by solid red circles in Figure 5b. The intensity, I_G/I_{RBM}, has the largest value at $\theta_1 - \theta_2 = 0°$ and 180°, falls almost to zero at $\theta_1 - \theta_2 = 60°$ and 120°, and has a local maximum at $\theta_1 - \theta_2 = 90°$. For comparison, the polarization dependence of graphite taken with the transient reflectivity measurement is also plotted with solid black circles in Figure 5b. As expected from E_{2g} Raman tensor of the G mode in graphite, the intensity shows a $|\cos(2(\theta_1 - \theta_2))|^2$ dependence.[26,29] The polarization dependence in Figure 5a looks similar to the polarized Raman spectroscopy of aligned nanotubes[19,37] for which the intensity in the *VV* geometry of the G band phonon mode with *A* symmetry has a minimum at 60° for the angle between the nanotubes axis and the polarization direction of light. This angular polarization dependence can be explained by a functional shape of nonresonant Raman tensor of the G band phonon mode with *A* symmetry.[19,37] In the present measurement, however, the *VV* geometry in the Raman measurement corresponds to the zero relative angle between the polarization directions of the pump and probe light. Thus, the origin of the present measurement should be different from the previous Raman measurement.

To characterize the polarization dependence in SWCNTs further, we investigated the dependence of the G mode

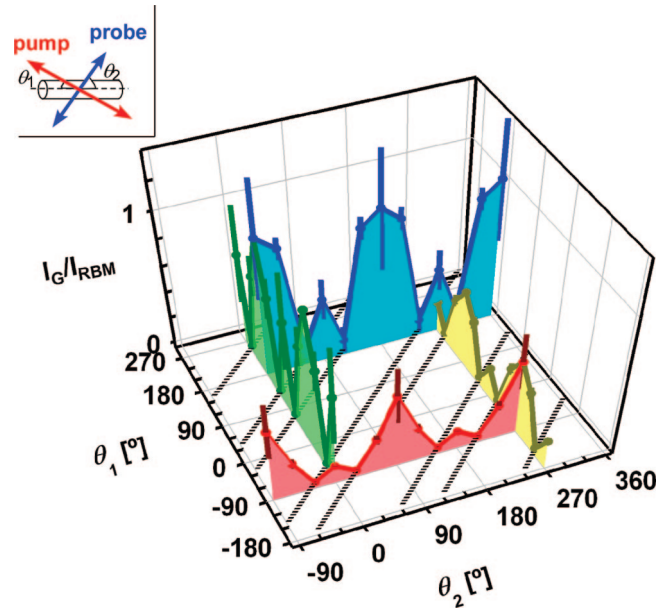

Figure 6. Polarization dependence of I_G/I_{RBM} plotted as a function of (θ_1,θ_2) where θ_1 (θ_2) is the angle of pump (probe) polarization with respect to the axis of SWCNTs. Dotted lines connect between points where I_G/I_{RBM} nearly equals zero.

intensity on angles θ_1 and θ_2. Figure 6 shows the intensity ratio between the G mode and the RBM, I_G/I_{RBM} plotted as a function of (θ_1, θ_2). In Figure 6, I_G/I_{RBM} strongly depends on the relative angle, $\theta_1 - \theta_2$. When the pump and probe

polarizations are parallel, that is, $|\theta_1 - \theta_2| = 0°$ or 180°, I_G/I_{RBM} is maximum, and when the relative angle between the pump and probe is $|\theta_1 - \theta_2| = 60°$ or 120°, I_G/I_{RBM} is zero (indicated by dotted lines in Figure 6). Furthermore, I_G/I_{RBM} has a local maximum when the pump and probe are perpendicular, that is, $|\theta_1 - \theta_2| = 90°$.

In order to discuss the observed G mode polarization dependence in Figures 5 and 6, we take into account the superposition of G band phonons with different symmetries. Such a superposition between phonons with different symmetries has been reported in GaAs/AlGaAs multiple quantum wells (MQWs),[38] in which they consider the summation of the corresponding Raman tensors.

In CNTs, when the excitation light propagates in the x direction with polarization vector in the z direction corresponding to the nanotube axis, C_6 symmetry Raman tensors with A, E_1, and E_2 symmetries in yz plane can be expressed as

$$A:\begin{pmatrix} a & 0 \\ 0 & b \end{pmatrix} \quad E_1:\begin{pmatrix} 0 & c \\ c & 0 \end{pmatrix} \quad E_2:\begin{pmatrix} d & 0 \\ 0 & 0 \end{pmatrix}$$

respectively (Table 1 in ref 39). Scattering efficiencies of the A, E_1, and E_2 symmetries are given by $|(a + b)/2 + (b - a)/2 \cos(2\theta)|^2$, $|c \cos(2\theta)|^2$,[26,38] and $|d(1 - \cos(2\theta))/2|^2$, respectively, where θ is the pump polarization. The polarization dependence of the E_{2g} symmetry phonon in graphite is well reproduced with $|\cos(2\theta)|^2$.[40] A previous polarized Raman measurement[36] in CNTs experimentally shows that the G mode with A symmetry has $a = 0$. Then, the scattering efficiency of the A symmetry phonon is $|b/2(1 + \cos(2\theta))|^2$. Neither the A nor the E symmetry Raman tensors alone can explain the present polarization dependence of CNTs with the minima at $\theta = 60°$ and 120°.

When all of the contributions from the A, E_1, and E_2 symmetries are taken, the total scattering intensity is given by

$$\frac{dS}{d\Omega} \propto |\alpha + \beta \cos(2\theta)|^2 \qquad (1)$$

where α and β combine the elements of the Raman tensors. Indeed, the observed polarization dependence in CNTs can be well-reproduced by eq 1 provided that $\alpha/\beta = 0.5$ (solid red line in Figure 5b). The G mode polarization dependence can be explained by the superposition of A, E_1, and E_2 symmetry Raman tensors.

In a previous polarized Raman measurement with the linearly and circularly polarized light,[41] the phonon symmetries of CNTs were investigated from the measurement of Raman tensor invariants. In that work, the ratio between the antisymmetric and the isotropic invariant shows that the Raman peaks of CNTs are not due to modes of distinctly different symmetry but are due to a superposition of the A and the E symmetry modes. Because our result also indicates the superposition between the A and the E symmetry modes, it corresponds to a real-time observation of the superposition of phonons with different symmetries. From the fact that the frequencies of the G band phonon are close to each other, the disappearance of the total G band phonon amplitude at certain angle in our time domain data suggests that the G band phonons with different symmetries might oscillate with different phases to give the observed angular dependence. Further understanding of the polarization dependence of the G mode excitation will require a detailed theoretical treatment.

In summary, we have studied coherent phonons in aligned bundles of SWCNTs with time-resolved reflectivity measurement. Through the time-resolved reflectivity measurements in the transient reflectivity or EO sampling geometries, we have observed coherent phonons of A and E symmetries. With the use of aligned bundles of SWCNTs, we have observed the strong polarization dependence of both the reflectivity and the amplitude of coherent phonons. The polarization dependence of the G mode taken by the transient reflectivity is explained by the superposition of the A and the E symmetry Raman modes.

Acknowledgment. K.K. would like to thank Dr. S. Nakashima and Dr. T. Kitamura for taking polarized Raman spectrum and Dr. M. Hase, Dr. O. V. Misochko, and Dr. A. Kubo for fruitful discussions. This research was supported by NIMS project research fund and Grants-in-Aid for Scientific Research (Nos. 18340093, 20750021, 20241023, and 16076201) from MEXT and JSPS, Ikerbasque, and NSF Grant CHE-0650756.

References

(1) Yao, Z.; Kane, C. L.; Dekker, C. *Phys. Rev. Lett.* **2000**, *84*, 2941–2944.
(2) Bachilo, S. M.; Strano, M. S.; Kitterell, C.; Hauge, R. H.; Weisman, R. E. S. R. B. *Science* **2002**, *298*, 2361–2366.
(3) Korovyanko, O. J.; Sheng, C.-X.; Vardeny, Z. V.; Dalton, A. B.; Baughman, R. H. *Phys. Rev. Lett.* **2004**, *92*, 017403.
(4) Wang, F.; Dukovic, C.; Brus, L. E.; Heinz, T. F. *Science* **2005**, *308*, 838–841.
(5) (a) Piscanec, S.; Lazzeri, M.; Mauri, F.; Ferrari, A. C.; Robertson, J. *Phys. Rev. Lett.* **2004**, *93*, 185503. (b) Piscanec, S.; Lazzeri, M.; Robertson, J.; Ferrari, A. C.; Mauri, F. *Phys. Rev. B.* **2007**, *75*, 035427.
(6) Sasaki, K.; Saito, R.; Dresselhaus,G.; Dresselhaus, M. S.; Farhat, H.; Kong, J. *Phys. Rev. B* 2008, *77*, 245441, related papers therein.
(7) Fagan, J. A.; Simpson, J. R.; Landi, B. J.; Richter, L. J.; Mandelbaum, I.; Bajpai, V.; Ho, D. L.; Raffaelle, R.; Walker, A. R. H.; Bauer, B. J.; Hobbie, E. K. *Phys. Rev. Lett.* **2007**, *98*, 147402.
(8) Lefebvre, J.; Finnie, P. *Phys. Rev. Lett.* **2007**, *98*, 167406.
(9) Murakami, Y.; Einarsson, E.; Edamura, T.; Maruyama, S. *Phys. Rev. Lett.* **2005**, *94*, 087402.
(10) Freitag, M.; Martin, Y.; Misewich, J. A.; Martel, R.; Avouris, P. *Nano Lett.* **2003**, *3*, 1067–1071.
(11) Saito, R.; Dresselhaus, G.; Dresselhaus, M. S. *Physical Properties of Carbon Nanotubes*; Imperial College Press: London, 1998.
(12) Jorio, A.; Filho, A. G. S.; Brar, V. W.; Swan, A. K.; Unlu, M. S.; Goldberg, B. B.; Righi, A.; Hafner, J. H.; Lieber, C. M.; Saito, R.; Dresselhaus, G.; Dresselhaus, M. S. *Phys. Rev. B* **2002**, *65*, 121402(R)
(13) Ajiki, H.; Ando, T. *Physica B* **1994**, *201*, 349–352.
(14) Wang, Y.; Kempa, K.; Kimball, B.; Carlson, J. B.; Benham, G.; Li, W. Z.; Kempa, T.; Rybczysnki, J.; Herczynski, A.; Ren, Z. F. *Appl. Phys. Lett.* **2004**, *85*, 2607–2609.
(15) Akturk, A.; Pennington, G.; Goldsman, N.; Wickenden, A. *IEEE Trans. Nanotech.* **2007**, *6*, 469–474.
(16) Jiang, J.; Saito, R.; Samsonidze, G. G.; Chou, S. G.; Jorio, A.; Dresselhaus, G.; Dresselhaus, M. S. *Phys. Rev. B* **2005**, *72*, 235408.
(17) Saito, R.; Jorio, A.; Filho, A. G. S.; Dresselhaus, G.; Dresselhaus, M. S.; Pimenta, M. A. *Phys. Rev. Lett.* **2002**, *88*, 027401.
(18) Saito, R.; Jorio, A.; Hafner, J. H.; Lieber, C. M.; Hunber, M.; McClure, T.; Dresellhaus, G.; Dresselhaus, M. S. *Phys. Rev. B* **2001**, *64*, 085312.
(19) Saito, R.; Takeya, T.; Kimura, T.; Dresselhaus, G.; Dresselhaus, M. S. *Phys. Rev. B* **1998**, *57*, 4145–4153.
(20) Jorio, A.; Dresselhaus, G.; Dresselhaus, M. S.; Souza, M.; Dantas, M. S. S.; Pimenta, M. A.; Rao, A. M.; Saito, R.; Liu, C.; Cheng, H. M. *Phys. Rev. Lett.* **2000**, *85*, 2617–2620.

(21) Fantini, C.; Pimenta, M. A.; Dantas, M. S. S.; Ugarte, D.; Rao, A. M.; Jorio, A.; Dresselhaus, G.; Dresselhaus, M. S. *Phys. Rev. B* **2001**, *63*, 161405.
(22) Jorio, A.; Pimenta, M. A.; Filho, A. G. S.; Samsonidze, G. G.; Swan, A. K.; Unlu, M. S.; Goldberg, B. B.; Saito, R.; Dresselhaus, G.; Dresselhaus, M. S. *Phys. Rev. Lett.* **2003**, *90*, 107403.
(23) Hase, M.; Kitajima, M.; Constantinescu, A. M.; Petek, H. *Nature* **2003**, *426*, 51–54.
(24) Misochko, O. V.; Ishioka, K.; Hase, M.; Kitajima, M. *J. Phys.: Condens. Matter* **2006**, *18*, 10571–10584.
(25) Dekorsy, T.; Auer, H.; Waschke, C.; Bakker, H. J.; Roskos, H. G.; Kurz, H. *Phys. Rev. Lett.* **1995**, *74*, 738–741.
(26) Yee, K. J.; Lee, K. G.; Oh, E.; Kim, D. S.; Lim, Y. S. *Phys. Rev. Lett.* **2002**, *88*, 105501.
(27) Gambetta, A.; Manzoni, C.; Menna, E.; Meneghetti, M.; Cerullo, G.; Lanzani, G.; Tretiak, S.; Piryatinski, A.; Ssaxena, A.; Martin, R. L.; Bishop, A. R. *Nature Phys.* **2006**, *2*, 515–520.
(28) Lim, Y.-S.; Yee, K.-J.; Kim, J.-H.; Haroz, E. H.; Shaver, J.; Kono, J.; Doorn, S. K.; Hauge, R. H.; Smalley, R. E. *Nano Lett.* **2006**, *6* (12), 2696–2700.
(29) Ishioka, K.; Kitajima, M.; Misochko, O. V. *J. Appl. Phys.* **2006**, *100*, 093501.
(30) Shimoda, H.; Oh, S. J.; Geng, H. Z.; Walker, R. J.; Zhang, X. B.; McNeil, L. E.; Zhou, O. *Adv. Mater.* **2002**, *14*, 899–901.
(31) Kim, Y.; Minami, N.; Kazoui, S *Appl. Phys. Lett.* **2005**, *86*, (073103)
(32) Ichida, M.; Mizuno, S.; Kataura, H.; Achiba, Y.; Nakamura, A. *Appl. Phys. A: Mater. Sci. Process.* **2004**, *78*, 1117–1120.
(33) Kataura, H.; Kumazawa, Y.; Maniwa, Y.; Umezu, I.; Suzuki, S.; Ohtsuka, Y.; Achiba, Y. *Synth. Met.* **1999**, *103*, 2555–2558.
(34) Asari, E.; Kitajima, M.; Nakamura, K. G.; Kawabe, T. *Phys. Rev. B* **1993**, *47*, 11143–11148.
(35) Hertel, T.; Fasel, R.; Moos, G. *Appl. Phys. A: Mater. Sci. Process.* **2002**, *75*, 449–465.
(36) Gommans, H. H.; Alldredge, J. W.; Tashio, H.; Park, J.; Magnuson, J.; Rinzler, A. G. *J. Appl. Phys.* **2000**, *88*, 2509.
(37) Rao, A. M.; Jorio, A.; Pimenta, M. A.; Dantas, M. S. S.; Saito, R.; Dresselhaus, G.; Dresselhaus, M. S. *Phys. Rev. Lett.* **2000**, *84*, 1820–1823.
(38) Yee, K. J.; Lim, Y. S.; Dekorsy, T.; Kim, D. S. *Phys. Rev. Lett.* **2001**, *86*, 1630–1633.
(39) Loudon, R. *Adv. Phys.* **2001**, *50*, 813–864.
(40) Ishioka, K.; Hase, M.; Kitajima, M.; Wirtz, L.; Rubio, A.; Petek, H. *Phys. Rev. B* **2008**, *77*, 121402(R)
(41) Reich, S.; Thomsen, C.; Duesberg, G. S.; Roth, S. *Phys. Rev. B* **2001**, *63*, 041401(R)

NL801200P